Cancer Immunology, Immunotherapy (2025) 74:190
https://doi.org/10.1007/s00262-025-04033-z

RESEARCH

Transcriptomic and proteomic characterization of cell and protein biomarkers of checkpoint inhibitor-induced liver injury

Changhua Ji[1] · Steven Kumpf[2] · Jessie Qian[2] · Joel D. Federspiel[3] · Mark Sheehan[2] · Darien Capunitan[2] · Edmond Atallah[4,5] · Stuart Astbury[4,5] · Seda Arat[2] · Elias Oziolor[2] · Mireia Fernandez Ocana[3] · Shashi K. Ramaiah[6] · Jane Grove[4,5] · Guruprasad P. Aithal[4,5] · Thomas A. Lanz[2]

Received: 27 January 2025 / Accepted: 24 March 2025

Abstract

Immune checkpoint inhibitors (ICI) targeting CTLA-4 and PD-1 have shown remarkable antitumor efficacy, but can also cause immune-related adverse events, including checkpoint inhibitor-induced liver injury (ChILI). This multi-omic study aimed to investigate changes in blood samples from treated cancer patients who developed ChILI. PBMCs were sequenced for by transcriptomic and T cell receptor repertoire (bulk and single-cell immune profiling), and extracellular vesicle (EV) enrichment from plasma was analyzed by mass spectroscopy proteomics. Data were analyzed by comparing the ChILI patient group to the control group who did not develop ChILI and by comparing the onset of ChILI to pre-ICI treatment baseline. We identified significant changes in T cell clonality, gene expression, and proteins in peripheral blood mononuclear cells (PBMCs) and plasma in response to liver injury. Onset of ChILI was accompanied by an increase in T cell clonality. Pathway analysis highlighted the involvement of innate and cellular immune responses, mitosis, pyroptosis, and oxidative stress. Single-cell RNA sequencing revealed that these changes were primarily found in select T cell subtypes (including CD8 + effector memory cells), while CD16 + monocytes exhibited enrichment in metabolic pathways. Proteomic analysis of plasma extracellular vesicles showed enrichment in liver-associated proteins among differentially expressed proteins. Interestingly, an increase in PBMC PD-L1 gene expression and plasma PD-L1 protein was also found to be associated with ChILI onset. These findings provide valuable insights into the immune and molecular mechanisms underlying ChILI as well as potential biomarkers of ChILI.
Trial registration number NCT04476563.

Keywords Checkpoint inhibitor · ChILI · Liver injury · Biomarker · PD-L1

Introduction

Immune checkpoint inhibitors (ICI) targeting CTLA-4 (cytotoxic T lymphocyte-associated protein 4) and PD-1 (programmed cell death 1) demonstrated antitumor efficacy in preclinical models and humans across several types of cancers [1–3]. These ICIs have become the cornerstones of

Guruprasad P. Aithal and Thomas A. Lanz have contributed equally to this work.

✉ Changhua Ji
jichanghua5@gmail.com

✉ Thomas A. Lanz
thomas.a.lanz@pfizer.com

[1] Drug Safety R&D, Pfizer Inc, 10777 Science Center Dr., La Jolla, CA 92121, USA

[2] Drug Safety R&D, Pfizer Inc, Eastern Point Rd, 274-3715A, Groton, CT 06340, USA

[3] Drug Safety R&D, Pfizer, Andover, MA, USA

[4] Nottingham Digestive Diseases Centre, Translational Medical Sciences, School of Medicine, University of Nottingham, Nottingham, UK

[5] NIHR Nottingham Biomedical Research Centre, Nottingham University Hospitals NHS Trust and the University of Nottingham, Nottingham, UK

[6] Drug Safety R&D, Pfizer, Cambridge, MA, USA

Published online: 03 May 2025

modern immunotherapy for a variety of cancer types that demonstrated promising durable responses. These T cell co-inhibitory pathways, or checkpoints, maintain desirable cellular immunity in the body. Disruption of these immune checkpoints can result in enhanced antitumor immune response but can also cause immune-related adverse events (irAE) affecting various organ/tissues including liver [4–6]. The incidence rate of checkpoint inhibitor-induced liver injury (ChILI) is 11.5 per 1000 person months; about 3% of patients treated with single agent develop ChILI, but this can reach as high as 32% when combination of ICIs are used [7].

CTLA-4 is primarily expressed on CD4 + and CD8 + T cells [8]. It competes with CD28 for binding to CD80/86—the second signal required for T cell activation. PD-1 plays a vital role in keeping T cell activity in check in the peripheral tissues through interaction with one of its ligands, PD-L1 or PD-L2 [9], thereby maintaining immunologic tolerance. The exact immune mechanisms of irAEs or ChILI have not been elucidated [5]. ChILI exhibits features of acute liver injury and clinically resembles idiosyncratic DILI and acute autoimmune hepatitis (AIH). ChILI has phenotypic and morphologic characteristics that are similar to autoimmune diseases [10]. An animal model of DILI was developed by inhibiting immune tolerance; acute liver injury occurred when PD-1(−/−) mice were treated with the combination of anti-CTLA-4 antibody and amodiaquine [11]. If the mechanism of action were to drive adverse events, then the determinants of efficacy should also be similar to those with adverse effect.

Early diagnosis and differentiation of ChILI from DILI and AIH would facilitate appropriate clinical management of ChILI. Various approaches have been explored to identify biomarkers associated with efficacy in ICI-treated patients, such as immunophenotyping [12–14], cytokine profiling [15, 16], immune-related transcriptional signature [17–23], TCR clonality [24, 25], and multiplex IHC [26–28]. In monkey and mouse models with dual inhibition of CTLA-4 and PD-1 pathways, activation, proliferation, and infiltration of T cells in affected tissues (e.g., heart or liver) were observed [21, 29]. Immune signatures in peripheral blood and tissue have been identified as associated with irAEs and ChILI in these models. In the mouse ChILI model, CD8 + T cells were essential since liver injury was abrogated when CD8 + T cells were depleted. Histological examinations revealed multi-focal infiltrates with necrotic hepatocytes surrounded by lymphocytes [29]. ChILI patients treated with ipilimumab and nivolumab displayed some similar liver pathological changes and immune cell features to this mouse model. Focal necrosis throughout the liver parenchyma with CD8 + T cell-rich mixed mononuclear infiltration was commonly observed in ChILI patients [10, 30].

In the current study, PBMCs were analyzed by T cell receptor (TCR) sequencing and RNAseq. Single-cell RNAseq was performed on a subset of samples. Extracellular vesicle (EV) enrichment was performed on plasma samples followed by tandem mass tag (TMT) mass spectroscopy (M/S) for unbiased proteomic analysis. Samples from subjects affected by ChILI were compared to both pre-treatment baseline and control subjects receiving ICI therapies that did not develop ChILI. Distinct changes at transcriptomic and proteomic levels that were associated with the onset of ChILI were observed and are discussed.

Methods

Patient population

The experimental design is summarized in Fig. 1. Patients with cancer where immune checkpoint inhibitor (ICI) treatment was indicated as the main therapy were prospectively recruited with informed consent (trial registration: NCT04476563) at Nottingham University Hospitals NHS Trust (NUH). Blood samples were collected prior to treatment with ICI (before checkpoint inhibitor; BC). If patients developed ChILI (13–233 days following start of treatment, median 61.5 days), a blood sample was taken at the visit at the time of liver injury (TOL) with acute manifestation of liver injury meeting previously defined clinical chemistry criteria [31]. Additional blood samples were taken for a subset of subjects at follow-up (FU) visits (FU1: 3–49 days after TOL, median 19 days; FU2: 10–62 days after TOL, median 23 days). In addition, ChILI subject samples were collected at TOL for which BC were not available. Cancer patients that did not develop ChILI or any other organ toxicity were followed up after 12 weeks with a second blood collection, and this group was followed as a non-ChILI control (AC). Whole blood was preserved in PAXgene tubes for subsequent RNAseq, and plasma was isolated from EDTA tubes for proteomic analysis. The patients included 15 males and 46 females with a median age of 60 years old (ranging from 30–88 years). Patient metadata, including cancer type, ICI regimen and any corticosteroid treatment, are summarized in Suppl Table 1.

RNA extraction

RNA was isolated from blood preserved in PAXgene tubes (Qiagen) using the PAXgene Blood RNA Kit (Qiagen) according to manufacturer's protocol. Full methods are detailed in the Data Supplement.

Sequencing library generation

RNA input was 100 ng for the Lexogen QuantSeq 3'mRNA-Seq Library Preparation kit for Illumina (FWD) (Lexogen,

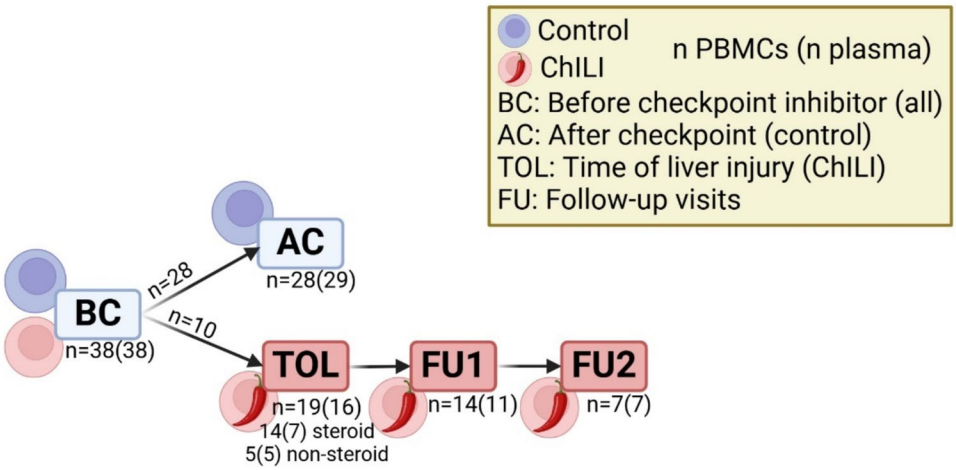

Fig. 1 Mixed prospective study experimental design. The various study groups are delineated by BC (before checkpoint inhibitor), AC (after checkpoint inhibitor control), TOL (time of liver injury), and FU (follow-up) timepoints 1 and 2. Under each group designation, the number of PBMC samples assessed for RNAseq is shown, followed by the number of plasma samples assessed by proteomics in parentheses. The numbers along the arrows indicate the number of patients in control and ChILI groups for whom BC samples were available. Additional ChILI subjects lacking BC samples were added to increase the power of the AC vs TOL comparison

#015.96) and libraries were prepared according to the manufacturer's protocol. After elution, libraries were quantified using the Qubit 4 Fluorometer (ThermoFisher Scientific, #Q33238) using the Qubit 1X dsDNA HS Assay Kit (ThermoFisher Scientific, #Q33231).

Bulk library sequencing

Libraries were sequenced either on an Illumina Nextseq 500 or Nextseq2K (Illumina, San Diego, CA) using a 75 cycle or 100 cycle single end flow cell, respectively.

Bulk TCR sequencing

For bulk human TCR RNA sequencing experiments, total RNA was normalized and used for TCR libraries generation using the SMARTer Human TCR-a/b Profiling kit v2 (Takara Bio Inc.) according to manufacturer's instructions. Libraries were sequenced on a MiSeq v3 (600 cycles) flow cell, targeting 5,000,000 read pairs per library.

Single-cell RNAseq

Single-cell RNAseq was performed by the 10 × Genomics single-cell 5′ Gene Expression and V(D)J library platform. Dead cells were removed using the Dead Cell Removal Kit (Miltenyi Biotec). Single-cell libraries were generated with Chromium Single Cell 5' Gene Expression and V(D)J Reagent Kit (10 × Genomics) per manufacturer's instruction. Purified libraries were sequenced on the Illumina NextSeq 2000 with 200 cycle kits.

TCR data analysis

Takara NGS Immune Profiler Software was utilized to process TCRseq samples in a conda base environment with python version 3.7.4. We used the *_cdr3_clones_results.csv files for diversity and clonality analysis [32]. The Gini coefficient was calculated to quantify clonality [33].

RNAseq data analysis

For bulk RNAseq data analysis, reads were pseudo-aligned to the *Homo sapiens* reference genome GRCh38.p14 from Ensembl v. 110 and quantified using Salmon version 1.10.0. Normalization factors were determined using the edgeR package (version 3.40.2) for expression data normalization and processing. Pairwise comparisons were run for differential expression, defined by timepoint (before and after checkpoint inhibitor) and outcome (ChILI and non-ChILI control). Benjamini–Hochberg multiple testing correction

was performed on p-values. Heatmaps were generated using the internally developed, publicly available application "HotGenes" (https://github.com/pfizer-opensource/Open-Hotgenes).

For single-cell RNAseq and V(D)J sequencing analysis, sequence reads were demultiplexed using CellRanger multi (10 × Genomics) and normalized, QC filtered and merged using the R package Seurat. Cell clusters were annotated using the human PBMC reference (HuBMAP Consortium), and differentially expressed genes within cell types in groups defined by timepoint and outcome were identified using the R package NEBULA. All RNAseq data have been uploaded to GEO (GSE287540, GSE287541).

Protein isolation and M/S

EV enrichment on patient plasma samples was performed using the Mag-Net method automated on a Kingfisher Apex as previously described [34]. The resulting peptides were then labeled with TMTpro reagents with a common pool of selected samples used as a bridge channel. Pooled TMT plexes were fractionated and analyzed by LC-MS^3 on an Eclipse Tribrid mass spectrometer using real-time search.

Protein data analysis

After instrument acquisition, data were analyzed on Proteome Discoverer 3.0. Raw protein abundance values were exported, bridge and global median normalization was performed, and resulting values were used for differential analysis with limma using sex as a factor. Proteins with Benjamini–Hochberg adjusted p-value of 0.1 or less were utilized for pathway analysis. All proteomic data have been uploaded to MassIVE (MSV000096928).

Secondary analysis and pathway enrichment

The Gini coefficients for TCR samples were plotted in GraphPad Prism (v10.2.1). For samples with BC data, Gini coefficients for subsequent visits were normalized to BC, and one-way ANOVA was performed in GraphPad using Sidak multiple comparison test.

For all differentially expressed transcripts and proteins (padj < 0.1; all raw *p*-values were < 0.05), gene IDs and corresponding p-values and fold changes were loaded into ingenuity pathway analysis (Qiagen). A comparison analysis was performed among all contrasts, and results were exported for enrichment of canonical pathways and upstream regulators. Common pathways were ranked by log(p-value) of enrichment and log2(fold change).

Results

ChILI is accompanied by an increase in T cell clonality

T cell receptor repertoires were assessed by profiling transcripts encoding TCRα and TCRβ subunits. Changes in clonality of TCR sequences were evaluated by calculating the Gini coefficient for each sample. The Gini coefficient is a measurement of the distribution of TCR sequences, ranging from 0 (maximum diversity) to 1 (maximum clonality) [35]. In subjects that developed ChILI, a trend toward increased clonality was observed in both TCRα and TCRβ from BC to TOL, which was reversed by FU2 in the few available FU2 samples (Fig. 2A and B). When samples were normalized to their respective BC time point, TOL samples were significantly elevated compared with both AC and FU time points (Fig. 2C and D), indicating a transient but significant increase in clonality in the T cell population in checkpoint inhibitor treated patients at the time of liver injury.

ChILI is associated with changes of gene expression in PBMCs

RNAseq data were analyzed for differences at various time points, between ChILI and control, and the impact of steroids (the full list of differentially expressed genes can be found in Suppl Table 2). The largest factor was found in subjects with PBMCs measured at TOL. A total of 554 differentially expressed genes (DEGs) were identified between TOL and BC, with 649 DEGs identified when comparing TOL with AC. A set of 261 DEGs (> 40%) were overlapping between the two contrasts. The top 50 DEGs between TOL and BC or AC are shown in Fig. 3. Most of the TOL samples cluster together, while AC and BC samples are intermixed. The majority of DEGs, as shown in red under the TOL samples, are upregulated at TOL relative to BC or AC. The top 20 DEGs between TOL or AC vs BC with fold changes and p-values are shown in Table 6 (found in Suppl). Comparing PBMC profiles in control subjects (those treated with ICI who did not develop liver injury), no changes in gene expression were observed between post-treatment (AC) to pre-treatment (BC). Therefore, the differentially expressed genes associated with TOL are likely indicative of the ChILI condition, and not the ICI treatment itself. One caveat in the TOL subjects was that a subset of these genes may also be impacted by steroid treatment; asterisks in Table 6 denote genes that were also statistically significant when comparing TOL patients on steroids to those who were not

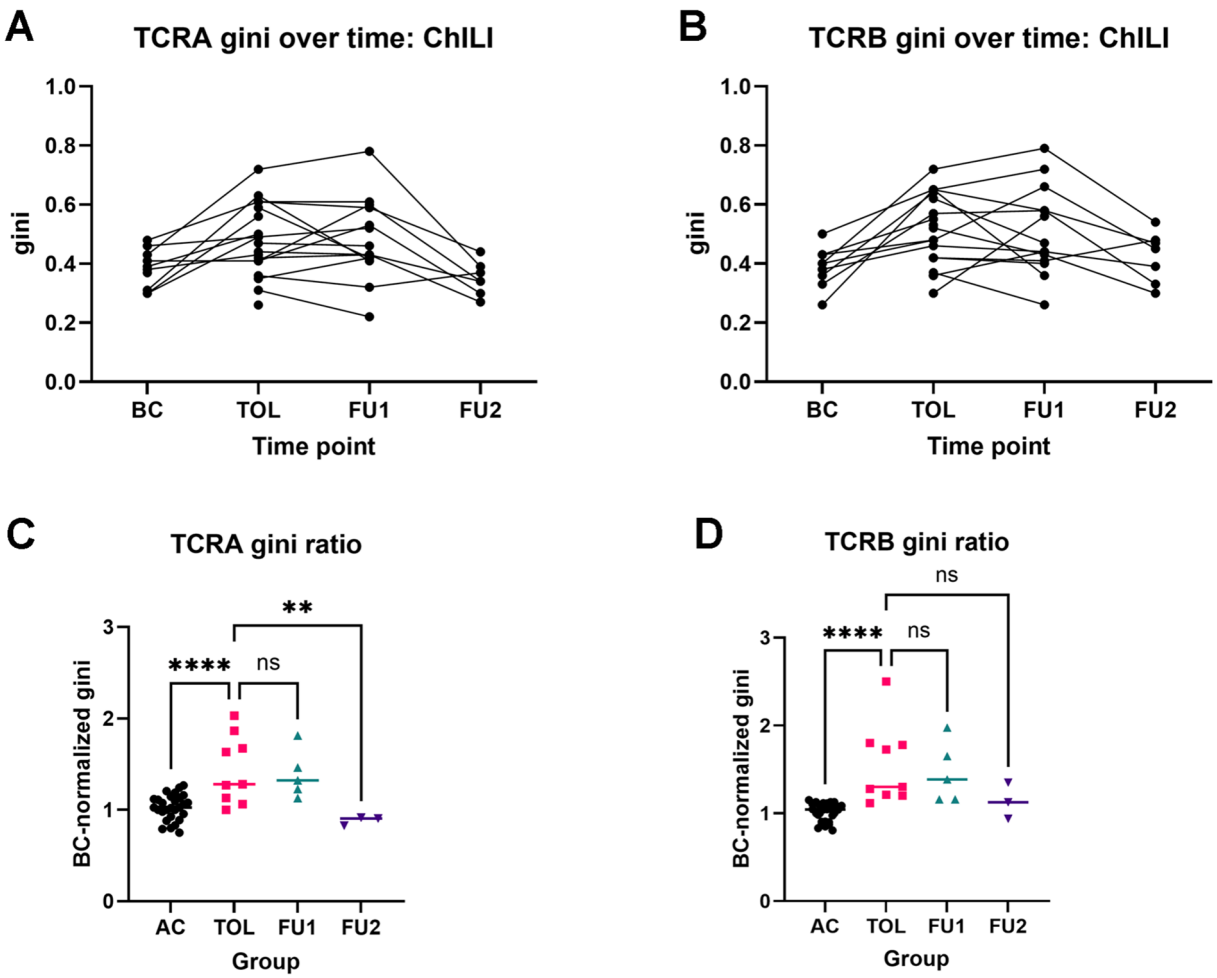

Fig. 2 T cell receptor clonality. Gini index was calculated for each sample. The Gini indices for TCRA (**A**) and TCRB (**B**) sequences are shown over time for subjects that developed ChILI. $^{*}p < 0.05$, $^{****}p < 0.0001$

on steroids. (A total of 191 DEGs were identified for this comparison; top 20 DEGs are shown in Suppl Table 3, with the full list available in Suppl Table 2) While many checkpoint inhibitor-related transcripts were unchanged across all contrasts, CD274 (the transcript encoding PD-L1) increased 1.47–2.12-fold in TOL vs AC and TOL vs BC comparisons, with no influence by steroid treatment. This increase could represent a persistent change due to feedback regulation following ICI inhibition.

To better understand the pattern of gene expression changes, pathway analysis was performed in ingenuity pathway analysis. The top 20 canonical pathways and predicted upstream regulators are shown in Table 1 (the full list of pathways for all contrasts is found in Suppl Table 4). These top 20 pathways/regulators primarily contain innate immune responses such as TLRs, type I IFN, NLR, and STING, and cellular immune response including MHC I antigen presentation and T cell effector response (TNF, IL17A, and IFNγ). As with DEGs, asterisks denote pathways also impacted in TOL subjects with versus without steroids. Common pathways with potential interaction by steroids included several inflammatory pathways, such as neutrophil degranulation, interleukin-1 family signaling, class I MHC-mediated antigen processing and presentation, and pathogen-induced cytokine storm signaling. Likewise, common upstream regulators predicted to be activated by TNF, IFNA, and IFNG were predicted to be inhibited by steroids, as would be expected. Several pathways implicated by ChILI DEGs related to mitosis, pyroptosis, and oxidative stress, however, were not enriched in the steroid vs no steroid comparison. While this suggests minimal impact of the steroids on reversing such pathways, and indeed a recent publication advocates a strategy that spares use of steroids [36], the smaller N for the steroid vs no steroid comparison is one caveat to this conclusion.

Additional contrasts compared the FU visits to TOL. Only 46 DEGs were identified for FU1 vs TOL, and 62 DEGs compared FU2 to TOL. No statistically significant

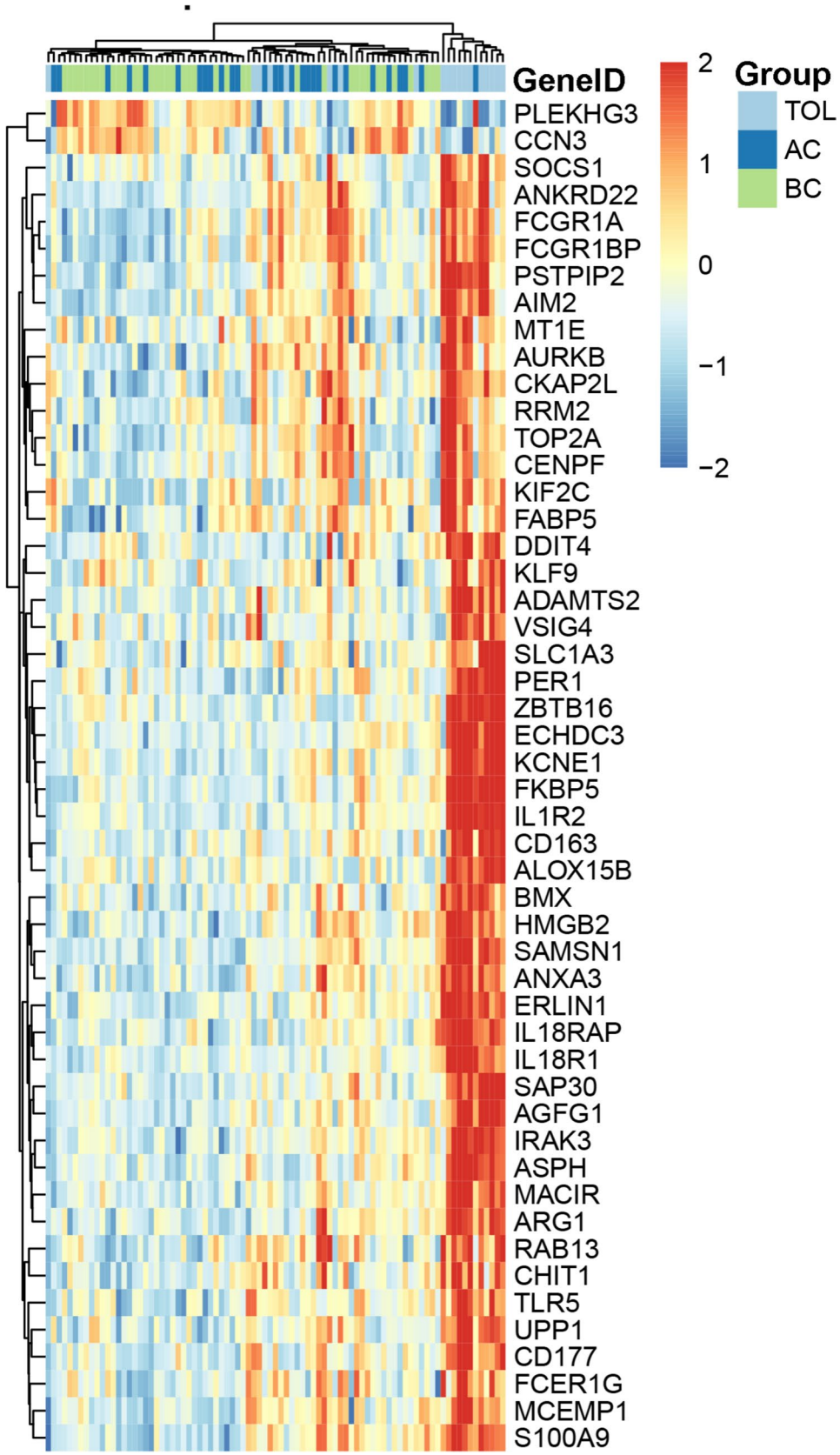

Fig. 3 Heatmap showing the top 50 differentially expressed genes among samples from TOL, AC and BC. Each column represents a single sample. Red represents up-regulation, blue represents down-regulation. In the top dendrogram, light blue represents TOL samples, dark blue represents AC samples, and green represents BC samples

Table 1 Top 20 pathways and upstream regulators in common between TOL vs BC and TOL vs AC contrasts enriched in RNAseq data

Canonical pathways	z-score		z-score		
	TOLvsBC	TOLvsAC	Upstream regulators	TOLvsBC	TOLvsAC
Neutrophil degranulation*	5.333	6.414	Lipopolysaccharide*	6.41	6.492
Mitotic G1 phase and G1/S transition	4.899	3.162	Filgrastim*	4.305	8.04
Mitotic metaphase and anaphase	4.491	2.496	poly rI:rC-RNA**	5.646	4.932
Synthesis of DNA	4.123	2.828	Interferon alpha**	5.396	5.16
Cachexia signaling pathway*	3.411	2.982	TNF**	4.975	4.791
Regulation of mitotic cell cycle	3.742	2.121	Dexamethasone*	2.592	6.888
Interleukin-1 family signaling*	3.742	2.111	Aflatoxin B1	5.425	4.017
Pyroptosis signaling pathway	2.5	3.317	IRF7**	4.998	4.045
Class I MHC-mediated antigen processing and presentation*	3.71	2.041	TBX3	4.845	4.079
Interferon gamma signaling	3.742	1.897	CEBPB	5.009	3.78
Pathogen-induced cytokine storm signaling pathway*	3.838	1.8	CSF2*	4.812	3.897
Neuroinflammation signaling pathway	3.317	2.111	Sirolimus	−4.456	−4.082
Role of chondrocytes in rheumatoid arthritis signaling pathway	2.828	2.53	Tetradecanoylphorbol acetate*	4.553	3.908
Oxidative stress-induced senescence	2.828	2.449	Metribolone	4.813	3.64
Neutrophil extracellular trap signaling pathway	3.545	1.606	TLR4	4.043	4.335
MyD88:MAL(TIRAP) cascade initiated on plasma membrane**	2.449	2.449	IFNG**	5.627	2.666
iNOS signaling	2.646	2.236	*E. coli* B4 lipopolysaccharide**	3.785	4.481
Sphingosine-1-phosphate signaling	−2.236	−2.53	STING1**	4.234	3.884
NLR signaling pathways	2.121	2.449	Eldr	4.359	3.742
Role of PKR in interferon induction and antiviral response	2.333	2.121	IL17A*	3.711	4.119

Single asterisks denote pathways or regulators that were significantly enriched with a positive z-score; double asterisks denote pathways or regulators that were significantly enriched with a negative z-score

pathways based on z-scores were identified for these contrasts. Another contrast within the BC group compared those subjects that would develop ChILI to those who did not, to look for potential risk factors ahead of treatment. Only four DEGs were identified between these two groups at baseline (MAML1, RPL10P9, PPP1R11, and HLA-DR2), and the fold changes were negligible (1.02–1.03).

Gene expression changes predominantly found in T cell subsets

To gain a higher resolution of the transcriptional changes following development of ChILI, PBMCs from a subset of patients (10 BC, 10 AC, 10 TOL, and 8 FU1) were evaluated by single-cell RNAseq. After separation of data from individual cell populations, most differentially expressed genes comparing post-treatment samples to BC in subjects who developed ChILI were identified as coming from CD8 + naïve T cells, CD16 + monocytes, CD8 + effector memory cells (TEM), and CD4 + central memory cells (TCM) (Fig. 4A). Many of the top pathways identified by bulk RNAseq, such as IFNg signaling, pathogen-induced cytokine storm signaling, and antigen presentation, were driven primarily by the T cell subtypes (Table 2). CD8 + TEM, CD8 Naive, and CD4 + TCM cells also showed enrichment in the T cell exhaustion signaling pathway. DEGs within CD16 + monocytes, conversely, were enriched for predominantly metabolic pathways. Despite monocytes being a prevalent cell type in PBMCs, enrichment of these metabolic pathways such as alanine biosynthesis, metabolism of water-soluble vitamins and cofactors, and GDP-L-fucose biosynthesis, were not detected in the bulk RNAseq data (Suppl Table 4).

Plasma proteomics revealed elevated liver proteins and inflammatory responses in ChILI patients

EV enrichment was performed on plasma for analysis of protein content by TMT LC-MS^3 based proteomics (Fig S1). Over 6,900 proteins were detected, with quantification of 3,758; 325 of these quantified proteins were found to be enriched in liver (Fig. 5A). Differentially expressed proteins (DEPs) were identified for TOL vs BC (319 DEPs) and TOL vs AC (261 DEPs). Across these comparisons, over 60% of the proteins with elevated expression in ChILI plasma were enriched for expression in liver (Fig. 5B and C).

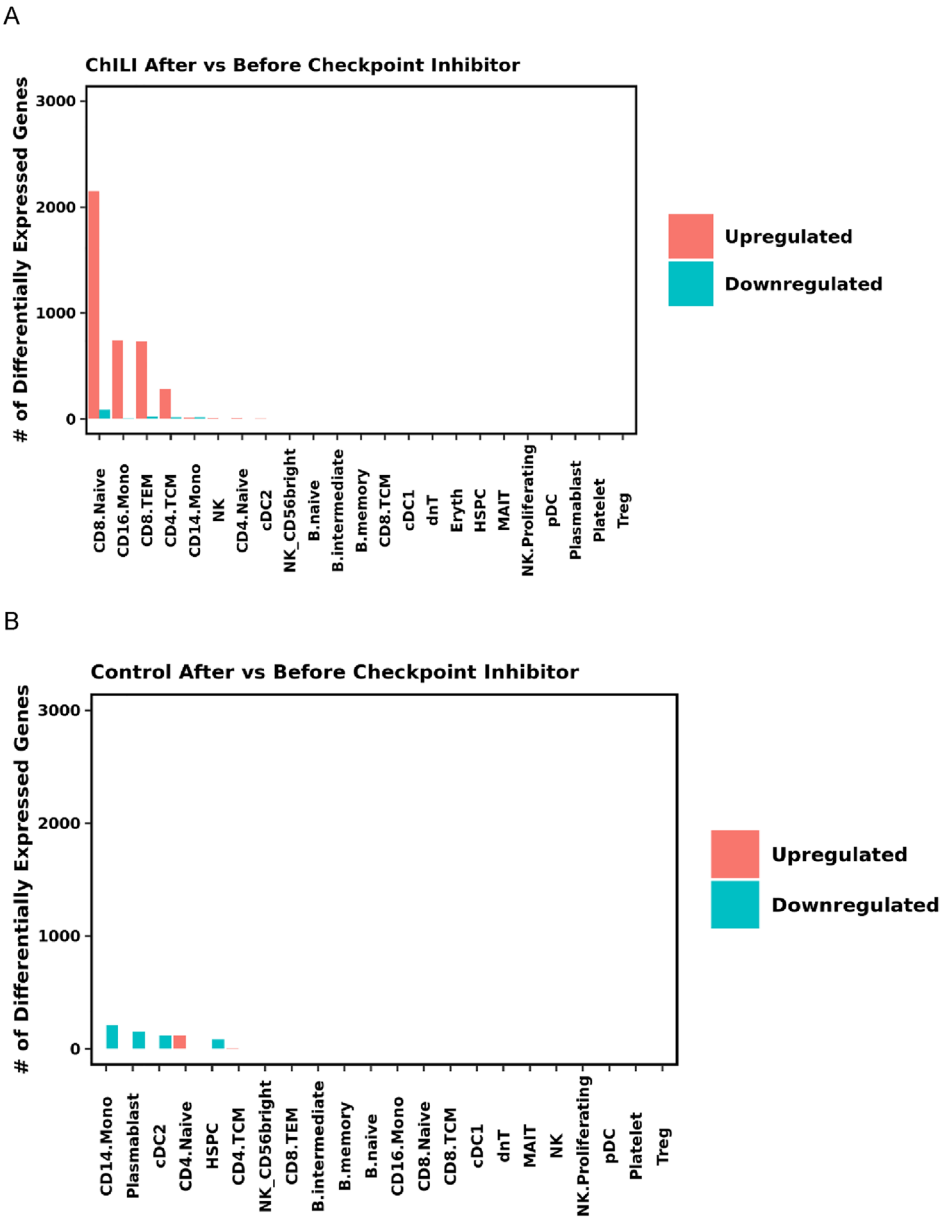

Fig. 4 Single-cell RNAseq. Number of DEGs in each of the cell types in PBMC comparing post-treatment to pre-treatment for those subjects that developed ChILI (**A**) and those subjects that did not develop ChILI (**B**)

Like the RNAseq results in PBMCs, the plasma proteomic data showed > 40% overlap in DEPs between the TOL vs BC and TOL vs AC contrasts, and no DEPs in the AC vs BC cohort. Unlike the RNAseq data, no DEPs were found to be associated with steroid treatment. Thus, the DEPs are likely not influenced by the steroid or ICI pharmacology but instead are a result of the ChILI condition. The top 20 DEPs in common between TOL vs BC and TOL vs AC are shown in Suppl Table 7 (found in Suppl) and includes several liver-enriched proteins involved various aspects of metabolism or functions, such as ALDOB, CPS1, ALDH1L1, GPT, BHMT, RBP4, POR, TTR, and GPT. At the onset of liver injury when compared with AC or BC, in addition to some of the liver-enriched enzymes (ALDOB, ALDH, CPS1, BHMT), there were also increases in sera in those proteins associated with tissue/cell injury (intracellular non-secreting proteins), such as STAT1, NCL, POR, PSMB8, API5, RSP20, and RPLP0.

Table 2 Top 10 pathways for ChILI post-treatment vs BC identified by single-cell RNAseq in CD16 monocytes, CD4 TCM, CD8 naïve T cells, or CD8 TEM cells

Canonical pathways	CD16 Mono	CD4 TCM	CD8 Naive	CD8 TEM
Pathogen-induced cytokine storm signaling pathway	0.40	**10.82**	**7.79**	0.98
Antigen presentation pathway	0.53	**7.38**	**8.87**	1.12
Th1 pathway	0.23	**8.83**	**5.09**	**2.25**
Th1 and Th2 activation pathway	0.00	**7.81**	**4.83**	**2.44**
Interferon gamma signaling	0.27	**6.57**	**3.00**	**5.18**
MHC class II antigen presentation	0.00	**4.76**	**7.09**	0.45
T Cell exhaustion signaling pathway	0.25	**5.89**	**2.78**	**3.08**
Th2 pathway	0.23	**7.39**	**3.43**	0.95
T helper cell differentiation	0.00	**6.94**	**1.96**	**1.97**
Metallothioneins bind metals	**5.25**	**1.58**	**3.66**	0.00
PD-1, PD-L1 cancer immunotherapy pathway	0.24	**6.27**	**2.89**	1.00
Costimulation by the CD28 family	0.28	**6.66**	**2.31**	0.59
B cell development	0.00	**6.04**	**2.94**	0.47
TCR signaling	0.00	**3.00**	**6.14**	0.00
FAT10 signaling pathway	0.00	0.54	**7.33**	0.27
Transcriptional regulation by RUNX1	0.00	0.28	**5.55**	**2.18**
RUNX1 and FOXP3 control the development of regulatory T lymphocytes (Tregs)	**1.26**	**1.49**	**1.83**	**2.67**
Actin cytoskeleton signaling	0.00	0.24	**6.86**	0.00
Response to elevated platelet cytosolic Ca2 +	0.00	0.42	**5.54**	0.00
RAF/MAP kinase cascade	0.00	0.20	**5.60**	0.00
SPINK1 general cancer pathway	**1.99**	**1.55**	**2.17**	0.00
Integrin signaling	0.00	0.00	**5.49**	0.00
Airway inflammation in asthma	0.00	**1.49**	0.94	**2.67**
Antimicrobial peptides	0.00	0.00	0.69	**3.97**
Amyloid fiber formation	0.47	0.67	0.57	**2.73**
Atherosclerosis Signaling	0.00	0.66	0.80	**2.68**
MyD88:MAL(TIRAP) cascade initiated on plasma membrane	0.00	0.00	0.43	**2.87**
Extracellular matrix organization	0.00	0.00	0.28	**2.99**
Interleukin-4 and Interleukin-13 signaling	**1.66**	0.00	0.72	0.73
Role of IL17A in Psoriasis	0.00	0.00	0.00	**2.89**
Metabolism of water-soluble vitamins and cofactors	1.88	0.00	0.35	0.32
Insertion of tail-anchored proteins into the endoplasmic reticulum membrane	**1.72**	0.00	0.00	0.61
Alanine biosynthesis III	**1.95**	0.00	0.00	0.00
Primary immunodeficiency signaling	**1.49**	0.00	0.44	0.00
Class I peroxisomal membrane protein import	**1.76**	0.00	0.00	0.00
GDP-L-fucose biosynthesis II (from L-fucose)	**1.65**	0.00	0.00	0.00
L-glutamine biosynthesis II (tRNA-dependent)	**1.65**	0.00	0.00	0.00

The given value is the $-\log(p\text{-value})$, and pathways are ranked by the sum across the four cell types. Significant enrichment (> 1.3) is denoted by bold

The full list of DEPs for all contrasts can be found in Suppl Table 2. Many proteins involved in the ICI response, such as CD27, CD28, CTLA-4 and PD-1, were not detected in the EV proteomic data. Like the PBMC RNAseq data, however, PD-L1 was significantly increased 1.75–1.90-fold in TOL vs AC and TOL vs BC contrasts.

Comparing the enriched pathways and upstream regulators for the proteomic data to the RNAseq data highlighted a clear role for innate immunity, interferon signaling, antigen presentation, and inflammatory responses (Table 3; Suppl Table 7). Enriched pathways predicted to be activated that were unique to the proteomic data included eukaryotic translation elongation, cellular

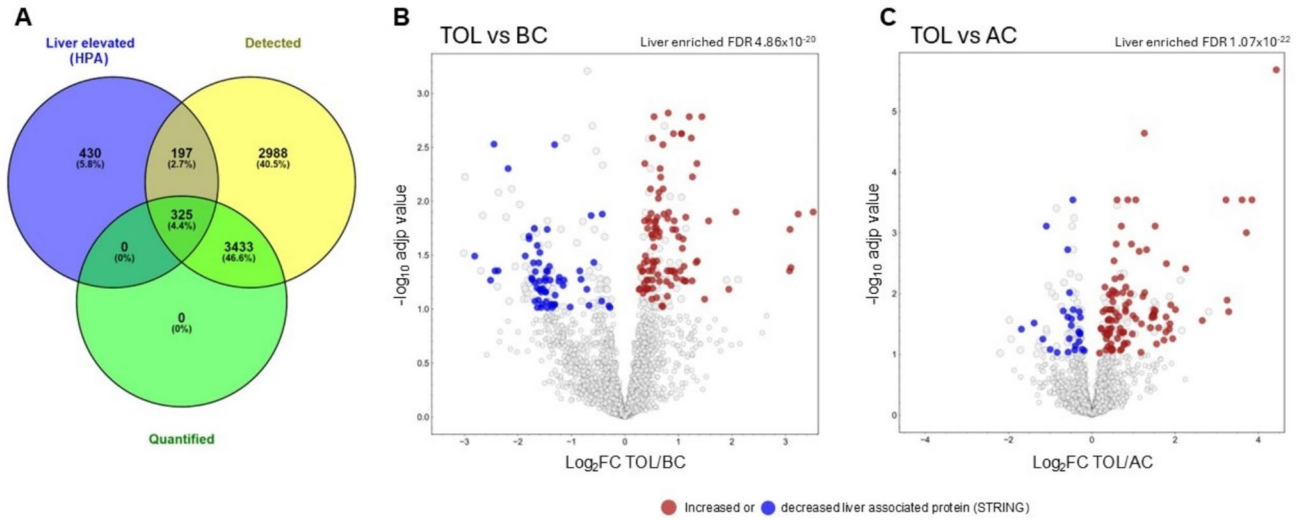

Fig. 5 Results of proteomic analysis of EV-enriched plasma. **A** Venn diagram depicting the overlap between total proteins detected, quantified, and those annotated as enriched in liver. Volcano plots highlighting the enrichment of liver-associated DEPs for **B** TOL vs BC and **C** TOL vs AC. Red circles denote increased expression, blue circles denote decreased expression of liver-associated proteins

Table 3 Top 20 pathways and upstream regulators in common between TOL vs BC and TOL vs AC contrasts enriched in proteomic data

Canonical pathways	z-score		z-score		
	TOL vs BC	TOL vs AC	Upstream regulators	TOL vs BC	TOL vs AC
Eukaryotic translation elongation	4.359	2.646	1,2-dithiole-3-thione	3.427	4.506
Cellular response to heat stress	2.646	2.646	sirolimus*	−3.131	−4.798
Interferon signaling*	2	2.236	IFNG*	3.417	4.457
ESR-mediated signaling	2	2.236	5-fluorouracil*	−3.492	−3.637
Chaperone mediated autophagy	−0.333	−2.985	MYCN*	3.431	3.349
Folate signaling pathway*	1.633	1.342	IRF7*	3.08	3.521
Amyloid fiber formation	−1.633	−1.342	MLXIPL	3.67	2.717
Role of JAK family kinases in IL-6-type cytokine signaling	1.134	1.633	STAT1	2.855	3.418
Superpathway of methionine degradation	1.342	1	3,5-dihydroxyphenylglycine	3.606	2.449
Aryl hydrocarbon receptor signaling*	−1	−0.447	USP8*	−2.626	−3.284
ISGylation signaling pathway	1.134	0	bortezomib*	2.607	3.278
Th17 activation pathway	−0.447	−0.447	lipopolysaccharide*	2.431	3.401
Xenobiotic metabolism AHR signaling pathway	0.378	0.447	SN-011*	−2.828	−2.828
			TREX1*	−2.828	−2.828
			KLF15*	2.789	2.758
			NKX2-3*	−2.53	−3
			IFNAR*	2.36	3.138
			CMTM3*	2.449	3
			IRF1*	2.191	3.236
			IL27*	2.428	2.969

Asterisks denote pathways or regulators in common between RNAseq and proteomic datasets

response to heat stress, and estrogen receptor signaling. The full list of pathways enriched by DEPs is available in Suppl Table 4.

Discussion

The present study sought to profile circulating biomarkers in patients impacted by ChILI using transcriptomic and

proteomic analyses. Blood samples were evaluated from prospectively enrolled cancer patients including those indicated for ICI before and during treatment, supplemented with additional post-treatment samples from ChILI patients and controls (ICI-treated subjects who did not develop ChILI). The results indicated that ChILI was accompanied by an increase in T cell clonality, and gene expression analysis revealed significant differences between ChILI and control subjects, particularly at the time of liver injury. Pathway analysis highlighted the involvement of innate and cellular immune responses, as well as pathways related to mitosis, pyroptosis, and oxidative stress. The single-cell RNA sequencing data showed that T cell subtypes primarily drove the identified pathways, while CD16 + monocytes exhibited enrichment in biosynthetic pathways, including alanine, GDP-L-fucose, L-glutamine and molybdenum cofactor biosynthesis. Proteomic analysis of plasma EVs revealed enrichment in liver-associated proteins among the differentially expressed proteins. The findings from both RNAseq and proteomics analyses highlight the activation of innate immunity, interferon signaling, antigen presentation, and associated inflammatory responses in ChILI.

The findings of increased clonality in ChILI subjects at TOL in the present study are consistent with expansion of antigen-specific T cells which may be involved in the liver injury. A single-cell RNA and TCR sequencing study of samples from patients dosed with ICI showed similar evidence of TCR clonotype expansion in patients experiencing myocarditis [37]. Other studies that have followed ICI-treated patients with single-cell TCR sequencing have observed early increases in T cell clonality in the absence of adverse tissue injury [38–40]. Early expansion of T cell clonality in circulating T cells as well as tumor-infiltrating T cells has been reported for oral cancer patients treated with ICI [41]. If an early increase in T cell clonality is a necessary component of ICI therapy, the difference in the present study in the cases of ChILI may either be a continued expansion that is propagated by other mechanisms, and it could be a secondary expansion as part of the reaction to a liver-specific antigen, or some combination thereof. Future studies profiling clonality changes over time would be necessary to ensure to provide a more comprehensive understanding of primary or secondary responses to therapy or tissue injury.

The majority of gene expression changes in the present study were found by comparing TOL to BC or AC; minimal changes were observed between AC and BC. A prior study in patients treated with ICI that developed myocarditis detected increases in multiple S100A family members by bulk RNAseq [39]. Aside from S100A9 (known to be involved in neutrophil chemotaxis and adhesion), which was elevated in TOL vs AC and TOL vs BC bulk RNAseq data, other S100A members were unchanged at the transcript or protein level in the present dataset. Another single-cell sequencing study also reported higher levels of effector T cells in patients experiencing myocarditis following ICI therapy [42]. Other studies have demonstrated significant impact of the ICI on PBMC immunophenotypes and gene expression. Single-cell RNAseq 1–3 weeks following treatment with ICI identified an increase in effector memory T cells and NK cells, accompanied by a reduction in B cells and CD4 + T cells, though these findings were in the absence of ChILI or myocarditis [38]. As the present data were typically collected at later time points during treatment, the T effector memory changes may be short-lived in response to treatment but may persist longer in subjects who develop ChILI. This highlights one of the limitations of this kind of study; the transcriptomic and proteomic data are collected at snapshots in time, while the underlying processes are dynamic. In the present study, however, the timing of the TOL samples (including FUs) is largely comparable to the AC control group.

The single-cell RNAseq data in the present study provided further information on ChILI-associated changes in specific populations of circulating immune cells. The changes in the CD8 + T effector memory cell population was previously identified in an overlapping set of ChILI samples to the present study by mass cytometry time of flight (CyTOF), and comparison to drug-induced liver damage and autoimmune hepatitis demonstrated specificity for this change in ChILI (Astbury et al., submitted manuscript). An increase in the CD8 + effector memory population was also detected by CyTOF and single-cell RNAseq in a cohort of ICI-treated patients with myocarditis [37], suggesting potentially common mechanisms underlying tissue injury due to a cell-mediated immune response. In a separate study of ICI patients with myocarditis, however, single-cell and bulk RNAseq also revealed changes in NK cells and B cells [39], which were not observed in the present study. None of the patients included here developed myocarditis, which is not surprising considering the low incidence (0.06–1%) of myocarditis compared to that of ChILI (8.8%) [7, 43].

The proteomic data generated in the present study used a new method focused on EV in plasma [34], and provided additional insight into the biology of ChILI. Specifically, a significant proportion of liver-associated proteins were found to be differentially elevated in subjects with ChILI, suggesting that proteomics identified potential biomarkers not restricted to circulating immune cells. In a recent study, some of these protein biomarkers such as Aldolase B and Carbamoyl-Phosphate Synthase 1 have been shown to be biomarkers that were able to distinguish DILI from acute non drug-induced liver injury [44]. A prior study used immuno-depletion of high abundance proteins in plasma followed by M/S proteomics in patients with ICI-associated myocarditis highlighted pathways related to innate immunity

and acute inflammatory response [42], but showed minimal overlap with the differential proteins identified in the present ChILI samples. This may imply that ChILI is not simply a consequence of the pharmacological action of ICI. A targeted analysis of checkpoint related proteins in exosomes from lung cancer patients 4–6 months after treatment with ICI revealed an increase in exosomal PD-L1 protein compared with healthy controls, but a reduction in PD-L1 protein in patients responding to therapy [45]. EV-associated PD-L1 protein can derive from tumor cells, some tissues, and circulating and tissue myeloid cells. In the present study, an increase in both gene expression in PBMC and EV-associated PD-L1 protein was observed for TOL compared to BC or AC groups, but no differences were seen solely due to therapy (AC vs BC). Since the increase in circulating PD-L1 protein is accompanied by an increase in PD-L1 gene expression in PBMC, circulating myeloid cells are one of the contributors of the increased production of and EV-associated PD-L1 protein in TOL. Hepatocytes constitutively express low level of PD-L1 which can increase significantly upon IFN stimulation therefore hepatocytes also contributed to the increased EV-associated PD-L1 in ChILI. This result suggests that increased expression of blood PD-L1 gene and protein can potentially serve as a biomarker of ChILI.

In summary, these results provide valuable insights into the immune and molecular mechanisms underlying ChILI in cancer patients. These data represent the first transcriptomic and proteomic analyses in a prospective cohort with adjudicated ChILI cases and control cancer patients. We found an increase in transcript encoding PD-L1 as well as EV-associated PD-L1 in association with TOL and may assist in the stratification of patients on ICI. One limitation to the present study is the relatively small sample size. Particularly when comparing FU1 and FU2 and when considering the steroid effects. While some impact of steroid treatment is clear, effect of steroids on certain pathways in ChILI patients cannot be completely ruled out. The small number of timepoints may not allow the capture of the full dynamic changes in T cell clonality. The use of a single pathway analysis tool simplifies analysis, but may also introduce some analytical bias. Re-analysis of these kinds of datasets and integration with other published datasets using foundational models or other similar artificial intelligence approaches may yield additional valuable insights. Another limitation is the lack of paired liver tissue evaluations to provide further insight at the tissue site and a more complete mechanistic picture of ChILI. The identification of ChILI-specific gene signatures and proteins, however, provides a source of novel potential biomarkers of ChILI that could be further validated in future exploratory clinical studies.

Supplementary Information The online version contains supplementary material available at https://doi.org/10.1007/s00262-025-04033-z.

Acknowledgements The authors are grateful to the study participants, the melanoma & renal cancer clinical nurse specialists at Nottingham University Hospitals NHS Trust and the team at NIHR Nottingham Biomedical Research Centre. The views expressed are those of the authors and not necessarily those of the NHS, the NIHR or the Department of Health. Figure 1 is created in Biorender (https://BioRender.com).

Author contributions Conceptualization was done by CJ and GPA; supervision administration and resources were done by SKR, GPA, JIG, MFO, and TAL; methodology was done by SK, JQ, JF, EA, and Stuart A; analysis was done by JF, MS, DC, Seda A, and EO. All authors reviewed the manuscript.

Funding Funding was provided by Pfizer Inc. EA, SA, JIG, and GPA are supported by NIHR Nottingham Biomedical Research Centre (NIHR203310).

Data availability All RNAseq data have been uploaded to GEO (https://www.ncbi.nlm.nih.gov/geo/): GSE287540, GSE287541. All proteomic data have been uploaded to MassIVE (https://massive.ucsd.edu/ProteoSAFe/static/massive.jsp): MSV000096928.

Declarations

Conflict of interest CJ, SK, JQ, JDF, MS, DC, Seda A, EO, MFO, SKR, and TAL are Pfizer employees.

References

1. Chen DS, Mellman I (2017) Elements of cancer immunity and the cancer-immune set point. Nature 541:321–330. https://doi.org/10.1038/nature21349
2. Prendergast GC, Malachowski WP, DuHadaway JB, Muller AJ (2017) Discovery of IDO1 inhibitors: from bench to bedside. Cancer Res 77:6795–6811. https://doi.org/10.1158/0008-5472.CAN-17-2285
3. Ribas A, Wolchok JD (2018) Cancer immunotherapy using checkpoint blockade. Science 359:1350–1355. https://doi.org/10.1126/science.aar4060
4. Larkin J, Chiarion-Sileni V, Gonzalez R et al (2015) Combined nivolumab and ipilimumab or monotherapy in untreated melanoma. N Engl J Med 373:23–34. https://doi.org/10.1056/NEJMoa1504030

5. Michot JM, Bigenwald C, Champiat S et al (2016) Immune-related adverse events with immune checkpoint blockade: a comprehensive review. Eur J Cancer 54:139–148. https://doi.org/10.1016/j.ejca.2015.11.016
6. Postow MA, Sidlow R, Hellmann MD (2018) Immune-related adverse events associated with immune checkpoint blockade. N Engl J Med 378:158–168. https://doi.org/10.1056/NEJMra1703481
7. Atallah E, Welsh SJ, O'Carrigan B et al (2023) Incidence, risk factors and outcomes of checkpoint inhibitor-induced liver injury: a 10-year real-world retrospective cohort study. JHEP Rep 5:100851. https://doi.org/10.1016/j.jhepr.2023.100851
8. Makarova-Rusher OV, Medina-Echeverz J, Duffy AG, Greten TF (2015) The yin and yang of evasion and immune activation in HCC. J Hepatol 62:1420–1429. https://doi.org/10.1016/j.jhep.2015.02.038
9. Boussiotis VA (2016) Molecular and biochemical aspects of the PD-1 checkpoint pathway. N Engl J Med 375:1767–1778. https://doi.org/10.1056/NEJMra1514296
10. Zen Y, Yeh MM (2018) Hepatotoxicity of immune checkpoint inhibitors: a histology study of seven cases in comparison with autoimmune hepatitis and idiosyncratic drug-induced liver injury. Mod Pathol 31:965–973. https://doi.org/10.1038/s41379-018-0013-y
11. Metushi IG, Hayes MA, Uetrecht J (2015) Treatment of PD-1(-/-) mice with amodiaquine and anti-CTLA4 leads to liver injury similar to idiosyncratic liver injury in patients. Hepatology 61:1332–1342. https://doi.org/10.1002/hep.27549
12. Martens A, Wistuba-Hamprecht K, Geukes Foppen M et al (2016) Baseline peripheral blood biomarkers associated with clinical outcome of advanced melanoma patients treated with ipilimumab. Clin Cancer Res 22:2908–2918. https://doi.org/10.1158/1078-0432.CCR-15-2412
13. Martens A, Wistuba-Hamprecht K, Yuan J et al (2016) Increases in absolute lymphocytes and circulating CD4+ and CD8+ T cells are associated with positive clinical outcome of melanoma patients treated with ipilimumab. Clin Cancer Res 22:4848–4858. https://doi.org/10.1158/1078-0432.CCR-16-0249
14. Simeone E, Gentilcore G, Giannarelli D et al (2014) Immunological and biological changes during ipilimumab treatment and their potential correlation with clinical response and survival in patients with advanced melanoma. Cancer Immunol Immunother 63:675–683. https://doi.org/10.1007/s00262-014-1545-8
15. Lou Y, Diao L, Cuentas ER et al (2016) Epithelial-mesenchymal transition is associated with a distinct tumor microenvironment including elevation of inflammatory signals and multiple immune checkpoints in lung adenocarcinoma. Clin Cancer Res 22:3630–3642. https://doi.org/10.1158/1078-0432.CCR-15-1434
16. Yamazaki N, Kiyohara Y, Uhara H et al (2017) Cytokine biomarkers to predict antitumor responses to nivolumab suggested in a phase 2 study for advanced melanoma. Cancer Sci 108:1022–1031. https://doi.org/10.1111/cas.13226
17. Bedognetti D, Wang E, Sertoli MR, Marincola FM (2010) Gene-expression profiling in vaccine therapy and immunotherapy for cancer. Expert Rev Vaccines 9:555–565. https://doi.org/10.1586/erv.10.55
18. Chifman J, Pullikuth A, Chou JW, Bedognetti D, Miller LD (2016) Conservation of immune gene signatures in solid tumors and prognostic implications. BMC Cancer 16:911. https://doi.org/10.1186/s12885-016-2948-z
19. Fehrenbacher L, Spira A, Ballinger M et al (2016) Atezolizumab versus docetaxel for patients with previously treated non-small-cell lung cancer (POPLAR): a multicentre, open-label, phase 2 randomised controlled trial. Lancet 387:1837–1846. https://doi.org/10.1016/S0140-6736(16)00587-0
20. Gentles AJ, Newman AM, Liu CL et al (2015) The prognostic landscape of genes and infiltrating immune cells across human cancers. Nat Med 21:938–945. https://doi.org/10.1038/nm.3909
21. Ji RR, Chasalow SD, Wang L et al (2012) An immune-active tumor microenvironment favors clinical response to ipilimumab. Cancer Immunol Immunother 61:1019–1031. https://doi.org/10.1007/s00262-011-1172-6
22. Tahara H, Sato M, Thurin M et al (2009) Emerging concepts in biomarker discovery; the US-Japan workshop on immunological molecular markers in oncology. j Transl Med 7:45. https://doi.org/10.1186/1479-5876-7-45
23. Ulloa-Montoya F, Louahed J, Dizier B et al (2013) Predictive gene signature in MAGE-A3 antigen-specific cancer immunotherapy. J Clin Oncol 31:2388–2395. https://doi.org/10.1200/JCO.2012.44.3762
24. Page DB, Yuan J, Redmond D et al (2016) Deep sequencing of T-cell receptor DNA as a biomarker of clonally expanded TILs in breast cancer after immunotherapy. Cancer Immunol Res 4:835–844. https://doi.org/10.1158/2326-6066.CIR-16-0013
25. Subudhi SK, Aparicio A, Gao J et al (2016) Clonal expansion of CD8 T cells in the systemic circulation precedes development of ipilimumab-induced toxicities. Proc Natl Acad Sci U S A 113:11919–11924. https://doi.org/10.1073/pnas.1611421113
26. Donnem T, Hald SM, Paulsen EE et al (2015) Stromal CD8+ T-cell density-A promising supplement to TNM staging in non-small cell lung cancer. Clin Cancer Res 21:2635–2643. https://doi.org/10.1158/1078-0432.CCR-14-1905
27. Roh W, Chen PL, Reuben A et al (2017) Integrated molecular analysis of tumor biopsies on sequential CTLA-4 and PD-1 blockade reveals markers of response and resistance. Sci Transl Med. https://doi.org/10.1126/scitranslmed.aah3560
28. Tsujikawa T, Kumar S, Borkar RN et al (2017) Quantitative multiplex immunohistochemistry reveals myeloid-inflamed tumor-immune complexity associated with poor prognosis. Cell Rep 19:203–217. https://doi.org/10.1016/j.celrep.2017.03.037
29. Llewellyn HP, Arat S, Gao J et al (2021) T cells and monocyte-derived myeloid cells mediate immunotherapy-related hepatitis in a mouse model. J Hepatol 75:1083–1095. https://doi.org/10.1016/j.jhep.2021.06.037
30. Kleiner DE, Berman D (2012) Pathologic changes in ipilimumab-related hepatitis in patients with metastatic melanoma. Dig Dis Sci 57:2233–2240. https://doi.org/10.1007/s10620-012-2140-5
31. Aithal GP, Watkins PB, Andrade RJ et al (2011) Case definition and phenotype standardization in drug-induced liver injury. Clin Pharmacol Ther 89:806–815. https://doi.org/10.1038/clpt.2011.58
32. Chiffelle J, Genolet R, Perez MA, Coukos G, Zoete V, Harari A (2020) T-cell repertoire analysis and metrics of diversity and clonality. Curr Opin Biotechnol 65:284–295. https://doi.org/10.1016/j.copbio.2020.07.010
33. Leydesdorff L (2018) Diversity and interdisciplinarity: how can one distinguish and recombine disparity, variety, and balance? Scientometrics 116:2113–2121
34. Wu CC, Tsantilas KA, Park J et al (2024) Mag-Net: rapid enrichment of membrane-bound particles enables high coverage quantitative analysis of the plasma proteome. bioRxiv. https://doi.org/10.1101/2023.06.10.544439
35. Bashford-Rogers RJ, Palser AL, Huntly BJ, Rance R, Vassiliou GS, Follows GA, Kellam P (2013) Network properties derived from deep sequencing of human B-cell receptor repertoires delineate B-cell populations. Genome Res 23:1874–1884. https://doi.org/10.1101/gr.154815.113
36. Riveiro-Barciela M, Barreira-Diaz A, Salcedo MT et al (2024) An algorithm based on immunotherapy discontinuation and liver biopsy spares corticosteroids in two thirds of cases of severe checkpoint inhibitor-induced liver injury. Aliment Pharmacol Ther 59:865–876. https://doi.org/10.1111/apt.17898

37. Zhu H, Galdos FX, Lee D et al (2022) Identification of pathogenic immune cell subsets associated with checkpoint inhibitor-induced myocarditis. Circulation 146:316–335. https://doi.org/10.1161/CIRCULATIONAHA.121.056730
38. Kim H, Park S, Han KY et al (2023) Clonal expansion of resident memory T cells in peripheral blood of patients with non-small cell lung cancer during immune checkpoint inhibitor treatment. J Immunother Cancer. https://doi.org/10.1136/jitc-2022-005509
39. Lou B, Guo M, Zheng T et al (2024) Single-cell RNA sequencing reveals the altered innate immunity in immune checkpoint inhibitor-related myocarditis. Immunology 172:235–251. https://doi.org/10.1111/imm.13770
40. Porciello N, Franzese O, D'Ambrosio L, Palermo B, Nistico P (2022) T-cell repertoire diversity: friend or foe for protective anti-tumor response? J Exp Clin Cancer Res 41:356. https://doi.org/10.1186/s13046-022-02566-0
41. Luoma AM, Suo S, Wang Y et al (2022) Tissue-resident memory and circulating T cells are early responders to pre-surgical cancer immunotherapy. Cell 185(2918–35):e29. https://doi.org/10.1016/j.cell.2022.06.018
42. Gao J, Wang Y, Lu L et al (2023) Peripheral immune mapping and multi-omics analysis in Pd-1 inhibitor-induced myocarditis. J Leukoc Biol 114:164–179. https://doi.org/10.1093/jleuko/qiad056
43. Ganatra S, Neilan TG (2018) Immune checkpoint inhibitor-associated myocarditis. Oncologist 23:879–886. https://doi.org/10.1634/theoncologist.2018-0130
44. Ravindra KC, Vaidya VS, Wang Z et al (2023) Tandem mass tag-based quantitative proteomic profiling identifies candidate serum biomarkers of drug-induced liver injury in humans. Nat Commun 14:1215. https://doi.org/10.1038/s41467-023-36858-6
45. Akbar S, Raza A, Mohsin R et al (2022) Circulating exosomal immuno-oncological checkpoints and cytokines are potential biomarkers to monitor tumor response to anti-PD-1/PD-L1 therapy in non-small cell lung cancer patients. Front Immunol 13:1097117. https://doi.org/10.3389/fimmu.2022.1097117